Minimising the energy consumption of tool change and tool path of machining by sequencing the features

Luoke Hu[a], Ying Liu[b,*](corresponding author), Chen Peng[a], Wangchujun Tang[c], Renzhong Tang[a], Ashutosh Tiwari[d]

[a]*State Key Laboratory of Fluid Power and Mechatronic Systems, School of Mechanical Engineering, Zhejiang University, Hangzhou, 310027, China*

[b]*School of Engineering, University of Glasgow, University Ave, Glasgow, G12 8QQ, United Kingdom*

[c]*Department of Mechanical and Aerospace Engineering, Syracuse University, Syracuse, NY 13244, United States*

[d]*Department of Automatic Control and Systems Engineering, The University of Sheffield, Sheffield, S1 3JD, United Kingdom*

***Corresponding author:** Ying Liu.
E-mail address: Ying.Liu@glasgow.ac.uk (Y. Liu).
Tel.: +44(0)7400028806; +44(0)7547650308.

Minimising the energy consumption of tool change and tool path of machining by sequencing the features

Abstract: A considerable amount of energy is consumed by machine tools during the run-time operations such as tool change and tool path. The value of this part of energy is affected by the processing sequence of features of a part (PSFP) because the tool path and tool change plan will vary based on the different PSFP. This paper firstly aims to understand the relationship between the PSFP and the energy consumption of tool change and tool path during the feature transitions. Then, a model is introduced for the single objective optimisation problem that minimises the energy consumption of machine tools during the feature transitions which include all the tool path and tool change operations. Finally, optimisation approaches including depth-first search and genetic algorithm are modified and applied to find the optimal PSFP which results in the minimisation of the energy consumption of feature transitions (EFT). In the case study, the optimal and near-optimal sequences of features, in terms of the minimum EFT, of a 15 features part which is processed by a machining centre have been found. The optimal PSFP achieves a 28.60% EFT reduction, which validates the effectiveness of the developed model and optimisation approaches. Besides, a 27.95% time reduction of feature transitions benefits from the EFT minimisation.

Keywords: Energy; Machine tools; Tool change and tool path; Feature sequencing; Depth-first search; Genetic algorithm

1. Introduction

To save cost and become environmentally friendly, reducing the energy consumption of production facilities is a new target for modern manufacturing companies [1]. Machine tools are widely used as the basic production facilities [2] in the manufacturing industry [3], and they are highly energy-intensive during production [4]. The statistics from the U.S. energy information administration showed that the electricity consumption of machine tools occupied above 10% of national consumption [5]. Therefore, reducing the energy consumption of machine tools (EMT) is a reasonable and significant routine to promote the manufacturing sustainability and alleviate the energy crisis [6].

Reducing the EMT is the goal of this paper. To achieve this goal, previous approaches have been developed to understand and characterise the EMT [7]. For example, Dahmus and Gutowski [8] and Kordonowy [9] broke the EMT in machining to three levels: the standby power, the run-time operations power and the actual cutting power [10]. The machine tools consume only the standby power during the idle mode [11]. This refers to the state of machine tools that the main power, computer panel and emergency stop are all switched on without load on any motors [12]. Run-time operations, including tool change and tool path (multiple axial feeding), enable the selected cutter to move to the right position to begin the actual cutting for the next step. By executing these operations, the power level of machine tools further increases because servo motors and spindle motors are all loaded. Finally, the actual cutting requires a further additional power [13]. Most existing research on reducing the EMT has been focused on actual cutting energy consumption [14] and standby energy consumption [15]. However, the understanding of characteristics of run-time energy consumption is limited in existing research, and the approaches to reduce this part of energy consumption have not been well explored. Especially, run-time energy consumption accounts for more than 35% of the total EMT during production [16], and it has energy-saving potentials. Thus, our research on reducing the EMT is focused on the run-time operations.

Adjusting the processing sequence of features of a part (PSFP) is an effective approach to reduce the EMT [17], and this approach is adopted in our paper. It has been proved that actual cutting energy consumption of a machine tool can be reduced by adjusting the PSFP [14]. However, existing research ignored run-time energy consumption when adjusting the PSFP [18]. Actually, the value of run-time energy consumption of a specific machine tool is also affected by the PSFP because the tool path for the cutter to reach the part for processing a specific feature and the corresponding tool change plan can vary when its preceding feature on the sequence is different [19]. This causes varying values of feeding power, feeding distance, feeding speed, and tool change time and power,

thereby resulting in the different value of total run-time energy consumption. It is the innovation of this paper to develop the mathematic relationship between the PSFP and the value of run-time energy consumption and then find the most energy-efficient PSFP.

Based on the above, our study firstly aims at understanding and characterising the EMT during run-time operations including tool path and tool change. Three sub-models have been developed to describe energy consumed by a machine tool while executing rapid and normal feeding activities and tool change. Based on the sub-models, a model to depict energy consumption during the tool change and tool path between processing a specific feature and its pre- or post- features has been further developed. This part of energy is defined as the energy consumption of feature transitions (EFT). The single objective optimisation in this research is to minimise the total EFT for processing a part by searching for the optimal PSFP. Depth-first search and genetic algorithm are modified and used as optimisation approaches. Based on a case study, the proposed model has been validated and the optimisation approaches are effective in finding the optimal or near-optimal processing sequences of features of a part (PSFPs). In this study, it is assumed that all of the required processing for a part can be finished on a single machine tool. If a part requires more than one machine tool to finish all of its features, the features to be processed on the same machine can be sorted and sequenced to reduce the EFT.

In the remainder of this paper, the literature review is presented in the next section. The description of the research problem and the model for minimising the EFT are given in Section 3. In Section 4, the working procedures of depth-first search and genetic algorithm for solving the aforementioned optimisation problem are described. A case study is conducted to demonstrate the developed model and optimisation approaches in Section 5. In Section 6, the effectiveness of this approach on the EFT reduction in multi-machine environment and a multi-objective model considering the EFT are discussed. Finally, a brief summary and future work are given in Section 7.

2. Literature review

Research has been developed to understand the relationship between the PSFP and the EMT. For example, Sheng et al. [14] developed a model to depict how the feature sequence of a part with three features (a groove, a hole and a planar face) to influence the value of cutting energy consumption. Wiener [20] investigated the EMT models for complex parts with more than 14 features. Srinivasan and Sheng [21] considered the manufacturing constraints such as the precedence relationships between features within a specific part. Further, a method to automatically identify features of a part

and generate energy-saving operations was developed by Yin et al. [18]. However, only the cutting energy consumption of machine tools has been considered in the aforementioned works while the EFT including the energy consumption of tool change and tool path has been ignored. Thus, the EFT model based on the PSFP is supplemented to bridge this knowledge gap.

Considerable amount of research has been focused on modelling the costs of tool change and tool path based on the PSFP. These can be used as references for our study to model the EFT. For example, Al-Sahib and Abdulrazzaq [22] and Abu Qudeiri et al. [23] studied the tool path cost based on a hole-making process. The corresponding problem for minimising the tool path cost by feature sequencing was formulated as a special case of travelling salesman problem, and the drilling time model was developed as well [24]. Kolahan and Liang [25] re-modelled the previous hole-making process by realising that the relevant cost minimisation problem was more complex than the travelling salesman problem because the cost associated with each drilling operation was both sequence-dependent and position-dependent. This single objective optimisation problem has also been formulated as a 0–1 non-linear mathematic model with consideration of tool air-cutting time and tool switch time [26]. For the tool change cost, a single objective optimisation problem for minimising it by feature sequencing was developed subjected to various manufacturing precedence constraints [27]. Bhaskara Reddy [28] proposed a feature precedence graph to identify manufacturing precedence constraints.

In above modelling research on the costs of tool change and tool path, there are mainly three limitations which weakened the accuracy of models: (1) It has been assumed that the costs for all tool change operations on a specific machine tool are same. However, in the reality, the tool change cost varies based on the number of station intervals rotated. (2) The tool path time was the single parameter to calculate the tool path cost. However, the tool path cost is affected by both the tool path time and the tool path cost per unit time. The latter one is a variable, changing its value based on process parameters such as feeding speed. (3) The data used for calculating the costs of tool change and tool path were subjectively assumed instead of experimentally measured on site. In the modelling work for the EFT, these weaknesses have been overcome by using the experimentally measured power data of machine tools and developing more precise models.

Both deterministic algorithms and meta-heuristics have been used as optimisation approaches to minimise the costs of tool change and tool path based on the PSFP. These can be used as references for our study to minimise the EFT. Normally, deterministic algorithms such as dynamic programming and branch-and-bound were employed to find the global optimum. However, these solutions

are more applicable for the small-to-medium sized problems with number of features less than 20. The computation time they consumed to find the global optimum sharply increases when solving the large sized problems [29]. Comparatively, meta-heuristics are able to provide the local or global optimum within much less computation time [30]. Therefore, they become increasingly popular to solve feature sequencing problems. Both types of solutions have been tested in our article. Specifically, depth-first search and genetic algorithm are selected as the optimisation approaches. When employing these approaches to minimise the EFT, several technical difficulties need to be overcome, such as the search tree generation for the EFT model. Finally, the optimisation results and computation time of developed approaches are validated and compared in the case study.

According to the relevant literatures reviewed, it can conclude that the EFT including energy consumption of tool change and tool path based on the PSFP has not been analysed and modelled. Further, optimisation approaches for reducing the EFT through adjusting the PSFP have not been explored yet. These knowledge gaps have negative impacts on the realisation of our goal to reduce the EMT. To bridge them, this paper develops a novel model to reflect the mathematic relationship between the PSFP and the EFT. Based on this model, depth-first search and genetic algorithm are first adopted to search for the PSFPs that result in the minimum EFT. The proposed solutions for modelling and optimising the EFT are main novelties and contributions of this paper, and they are introduced in the following sections.

3. Problem statement and modelling

The notation used in the problem statement, algorithm description and throughout the paper is as follows:

	Feature sequencing problem
i, k, j	indices for features of a part, positions in a PSFP and feeding activities in a feature transition
F_i	i-th feature of a part
F_C	a finite set of n features of a part, $F_C = \{F_i\}_{i=1}^{n}$
F	a finite set of $n+2$ features of a part within machining environment, $F = \{F_i\}_{i=0}^{n+1}$, $F_C \subset F$
F_0	a virtual feature to denote the start position of tools in machining
F_{n+1}	a virtual feature to denote the end position of tools in machining
S_k	k-th position of a sequence
S	a finite set of $n+2$ positions in a PSFP, $S = \{S_k\}_{k=1}^{n+2}$
m	number of feeding activities in a feature transition

Energy consumption

E_{FS}	total EFT based on a specific PSFP [J]
$E_{FT}^{(F_p,F_q)}$	EFT from the feature F_p to its post-feature F_q [J]
$E_{TC}^{(F_p,F_q)}$	energy consumption of tool change in the feature transition from F_p to F_q [J]
$E_{TP}^{(F_p,F_q)}$	energy consumption of tool path in the feature transition from F_P to F_q [J]
$E_{FT}^{(S_k,S_{k+1})}$	EFT from the feature at the k-th position to the feature at the $k+1$-th position of a sequence [J]
A	a finite set of energy consumption of m feeding activities $A=\left\{A_j^{(F_p,F_q)}\right\}_{j=1}^{m}$ during the feature transition from F_p to F_q, $(0\le p\le n, 1\le q\le n+1, p\ne q)$
$A_j^{(F_p,F_q)}$	energy consumption of the j-th feeding activity of the feature transition from F_p to F_q [J]
ΔX_j^{pq}, ΔY_j^{pq}, ΔZ_j^{pq}	relative distances between the start and end coordinate positions of X-axis, Y-axis and Z-axis in the j-th feeding activity of the feature transition from F_p to F_q [mm]
x_{j-1}^{pq}, x_j^{pq}	start and end coordinate value of X-axis in the j-th feeding activity of the feature transition from F_p to F_q [mm]
P_{SRj}^{pq}	spindle rotation power in the j-th feeding activity of the feature transition from F_p to F_q [W]
n_{SRj}^{pq}	spindle rotation speed in the j-th feeding activity of the feature transition from F_p to F_q [rpm]
P_{XFj}^{pq}, P_{YFj}^{pq}, P_{ZFj}^{pq}	feeding power of X-axis, Y-axis and Z-axis in the j-th feeding activity of the feature transition from F_p to F_q [W]
v_{XFj}^{pq}	feeding speed at the X-axis in the j-th feeding activity of the feature transition from F_p to F_q [mm/min]
v_j^{pq}	feeding speed in the j-th feeding activity of the feature transition from F_p to F_q [mm/min]
f_j^{pq}	feed rate in the j-th feeding activity of the feature transition from F_p to F_q [mm/r]
P_{TC}^{pq}	power of tool changer in the feature transition from F_p to F_q [W]

Time consumption

t_{XRj}^{pq}, t_{YRj}^{pq}, t_{ZRj}^{pq}	rapid feeding time of X-axis, Y-axis and Z-axis in the j-th feeding activity of the feature transition from F_p to F_q [s]
t_{ARj}^{pq}	axial rapid feeding time in the j-th feeding activity of the feature transition from F_p to F_q [s]
t_{AFj}^{pq}	axial feeding time in the j-th feeding activity of the feature transition from F_p to F_q [s]
$T_{TC}^{(F_p,F_q)}$	tool change time in the feature transition from F_p to F_q [s]
T_{FS}	total time consumption of feature transitions based on a specific PSFP [s]
$T_{FT}^{(S_k,S_{k+1})}$	time consumption of feature transitions from the feature at the

	k-th position to the feature at the $k+1$-th position of a sequence [s]
$T_{TP}^{(F_p,F_q)}$	time consumption of tool path in the feature transition from the feature F_p to its post-feature F_q [s]
$B_j^{(F_p,F_q)}$	time consumption of the j-th feeding activity of the feature transition from F_p to F_q [s]
	Machine tool related parameters
P_{XR}, P_{YR}, P_{ZR}	rapid feeding power of *X*-axis, *Y*-axis and *Z*-axis [W]
P_{ZR}^U, P_{ZR}^D	upward and downward rapid feeding power of *Z*-axis [W]
A_{XF}, A_{YF}	quadratic coefficient in the *X*-axial and *Y*-axial feeding power models
A_{ZF}^D, A_{ZF}^U	quadratic coefficient in the *Z*-axial downward and upward feeding power models
B_{SR}	monomial coefficient in the spindle rotation power model
B_{XF}, B_{YF}	monomial coefficient in the *X*-axial and *Y*-axial feeding power models
B_{ZF}^D, B_{ZF}^U	monomial coefficient in the *Z*-axial downward and upward feeding power models
C_{SR}	constant in the spindle rotation power model
P_0	standby power of a machine tool [W]
v_{XR}, v_{YR}, v_{ZR}	rapid feeding speed of *X*-axis, *Y*-axis and *Z*-axis [m/min]

Considering a part, all of its n actual features can be denoted as a finite set $F_C = \{F_i\}_{i=1}^{n}$. While machining the part, the total EFT is not only affected by the sequence of the actual features but also the start and end positions of tools. Hence, they are defined as two virtual features for the part, denoted by F_0 and F_{n+1}, respectively. In this machining background, there is a finite set of $n+2$ features $F = \{F_i\}_{i=0}^{n+1}$ for an n-features part. The F_C is a subset of the F ($F_C \subset F$). In terms of optimisation, the aim is to determine the optimal PSFP which results in the minimisation of the total EFT under precedence constraints.

As illustrated in **Fig. 1**, a part with two features (F_1 and F_2) is used as an example to show different PSFPs can result in different values of the total EFT. The two features are to be processed by two different drilling tools. The start and end positions of tools are virtual features which are denoted by F_0 and F_3, respectively. Therefore, F_0-F_1-F_2-F_3 and F_0-F_2-F_1-F_3 are the two PSFPs which can be used. Tool paths of the two PSFPs are labelled by blue solid lines and red dashed lines, respectively, in **Fig. 1**. A typical tool path is consisted of several feeding activities. For instance, the tool path from F_1 and F_2 includes four feeding activities: R_3, R_4, R_5 and N_6. "R" and "N" here are used to represent rapid feeding and normal feeding. These are the two potential feeding approaches to complete a specific feeding activity.

Fig. 1. A 2-feature part that has two feasible processing sequences.

Fig. 2. Power profiles of two sequences: (a) F_0-F_1-F_2-F_3; (b) F_0-F_2-F_1-F_3.

The corresponding power input model of a machine tool when processing the part according to the aforementioned two sequences are shown in **Fig. 2(a)** and **(b)**, respectively. The input power which a machine requires over time is defined as a stepped function represented by the solid black line in **Fig. 2**. It can be divided to constant power (standby) [9] and variable power [31]. The standby power is denoted as P_0. The variable power level during tool path is the sum of power of axial feeding and spindle rotation. The power of tool changer is also a variable. In **Fig. 2,** the areas filled with blue and red slashes and nets represent energy consumption of the machine during tool path; the yellow grids areas represent energy consumption of the machine during tool change; the blank areas represent energy consumption during actual cutting. Thus, the total EFT based on a specific PSFP is the coloured areas in either **Fig. 2(a)** or **Fig. 2(b)**. The EFT from finishing cutting the feature F_p to the beginning of cutting its post-feature F_q on the sequence can be expressed as:

$$E_{FT}^{(F_p,F_q)} = E_{TP}^{(F_p,F_q)} + E_{TC}^{(F_p,F_q)} \quad (1)$$

where $E_{FT}^{(F_p,F_q)}$, $E_{TP}^{(F_p,F_q)}$ and $E_{TC}^{(F_p,F_q)}$ $(0 \le p \le n, 1 \le q \le n+1, p \ne q)$ are the energy consumption of feature transitions, tool path and tool change, respectively, from the feature F_p to its post-feature F_q. The developed models for $E_{TP}^{(F_p,F_q)}$ and $E_{TC}^{(F_p,F_q)}$ are presented in Sections 3.1 and 3.2. By comparing the sizes of the coloured areas in **Fig. 2(a)** and **(b)**, it shows that different PSFPs may result in different values of the total EFT.

Following the example above, this research aims at searching for the optimal processing sequence of features for an n-feature part in terms of the minimisation of the total EFT. Considering there are $n+2$ features for an n-feature part in machining environment, a finite set of $n+2$ positions $S = \{S_k\}_{k=1}^{n+2}$ is employed to indicate the positions in a sequence. S_k indicates the k-th position of a sequence. For example, $S_k = F_p$ means the feature F_p is located at the k-th position of a sequence. For any part, F_0 is located at the 1-st position ($S_1 = F_0$) and F_{n+1} is located at the $n+2$-th position ($S_{n+2} = F_{n+1}$). Then, the objective function for minimising the total EFT based on a specific PSFP (E_{FS}) can be expressed as:

$$minimise\ E_{FS} = \sum_{k=1}^{n+1} E_{FT}^{(S_k,S_{k+1})} \quad (2)$$

where $E_{FT}^{(S_k,S_{k+1})}$ is the EFT between processing the feature at the k-th position and the feature at the $k+1$-th position of a sequence, which can be calculated according to Expression (1). Constraints of the model are developed according to the precedence constraints among features [29]. A feasible PSFP, namely, a feasible solution for the mathematic model, must satisfy all of the constraints. The total EFT for the corresponding PSFP is set to infinity "∞" once any feature and its pre- or post- feature in a sequence violate any constraint.

3.1. Modelling tool path energy consumption

It can be assumed that a tool path in the feature transition from the feature F_p to the feature F_q consists of m sequential feeding activities. Then, the energy consumption of the j-th feeding activity can be denoted as $A_j^{(F_p,F_q)}$. The tool path energy consumption portion of the EFT in a feature transition ($E_{TP}^{(F_p,F_q)}$) equals to the sum of energy consumption of all feeding activities, which can be expressed as:

$$E_{TP}^{(F_p,F_q)} = \sum_{j=1}^{m} A_j^{(F_p,F_q)}. \tag{3}$$

Considering there are two possible feeding approaches (rapid and normal) for the j-th feeding activity, two types of models for $A_j^{(F_p,F_q)}$ are provided in Sections 3.1.1 and 3.1.2.

3.1.1. Energy consumption of a rapid feeding activity

During a rapid feeding activity, the *X*-axis, *Y*-axis and *Z*-axis of the machine tool feed from the start to the end coordinate position with their maximum feeding speeds [16]. Therefore, the values of feeding time of the three axes are probably different. The rapid feeding power is consisted of rapid feeding power of *X*-axis, *Y*-axis and *Z*-axis, standby power and spindle rotation power [32]. Thus, the energy consumption of the j-th feeding activity ($A_j^{(F_p,F_q)}$) can be modelled as follow when using the rapid feeding approach:

$$A_j^{(F_p,F_q)} = [P_{XR} \quad P_{YR} \quad P_{ZR}] \times \left[t_{XRj}^{pq} \quad t_{YRj}^{pq} \quad t_{ZRj}^{pq}\right]^{\mathrm{T}} + \left(P_0 + P_{SRj}^{pq}\right) \times t_{ARj}^{pq} \tag{4}$$

where $[P_{XR} \quad P_{YR} \quad P_{ZR}]$ is the axial rapid feeding power vector, and P_{XR}, P_{YR} and P_{ZR} represent the rapid feeding power of *X*-axis, *Y*-axis and *Z*-axis, respectively. P_{XR} and P_{YR} are constants for a specific machine tool. For the *Z*-axis, the power used to drive the upward and downward rapid feedings

are different, which are denoted by P_{ZR}^{U} and P_{ZR}^{D}, respectively. $\left[t_{XRj}^{pq} \quad t_{YRj}^{pq} \quad t_{ZRj}^{pq}\right]$ is the axial rapid feeding time vector, and t_{XRj}^{pq}, t_{YRj}^{pq} and t_{ZRj}^{pq} are the rapid feeding time of the three axes. The vector can be calculated by:

$$\left[t_{XRj}^{pq} \quad t_{YRj}^{pq} \quad t_{ZRj}^{pq}\right] = \left[\frac{\Delta X_j^{pq}}{v_{XR}} \quad \frac{\Delta Y_j^{pq}}{v_{YR}} \quad \frac{\Delta Z_j^{pq}}{v_{ZR}}\right] \tag{5}$$

where v_{XR}, v_{YR} and v_{ZR} are the maximum feeding speeds [m/min] of the three axes. ΔX_j^{pq}, ΔY_j^{pq} and ΔZ_j^{pq} are the relative distances between the start coordinate position $(x_{j-1}^{pq}, y_{j-1}^{pq}, z_{j-1}^{pq})$ and the end coordinate position $(x_j^{pq}, y_j^{pq}, z_j^{pq})$ of the j-th feeding activity, as shown in **Fig. 1**. Thus, $\Delta X_j^{(F_p,F_q)} = \left|x_j^{pq} - x_{j-1}^{pq}\right|$, $\Delta Y_j^{(F_p,F_q)} = \left|y_j^{pq} - y_{j-1}^{pq}\right|$ and finally $\Delta Z_j^{(F_p,F_q)} = \left|z_j^{pq} - z_{j-1}^{pq}\right|$.

During the feeding activity, the machine consumes standby power P_0 and the spindle rotation is also on-state. These two portions of energy consumption also need to be counted in. Comparing several available models [32] to calculate spindle rotation power, the linear model proposed by Lv et al. [33] provides the highest accuracy which is 95%. Thus, this model is employed to calculate spindle rotation power of a machine tool in the j-th feeding activity (P_{SRj}^{pq}) as:

$$P_{SRj}^{pq} = B_{SR} \times n_{SRj}^{pq} + C_{SR} \tag{6}$$

where n_{SRj}^{pq} is spindle rotation speed [rpm] in the j-th feeding activity; coefficient B_{SR} and constant C_{SR} can be obtained by linear regression based on experiment data [33]. Finally, t_{ARj}^{pq} is axial rapid feeding time for the j-th feeding activity which is the maximum among the rapid feeding time of three axes that $t_{ARj}^{pq} = \max\{t_{XRj}^{pq}, \quad t_{YRj}^{pq}, \quad t_{ZRj}^{pq}\}$.

3.1.2. Energy consumption of a normal feeding activity

During a normal feeding activity, the feeding route is a straight line from the start to the end coordinate position [16]. Normal feeding power is the sum of feeding power of the three axes, spindle rotation power and standby power [32]. The energy consumption of the j-th feeding activity ($A_j^{(F_p,F_q)}$) can be modelled as follow when using the normal feeding approach:

$$A_j^{(F_p,F_q)} = \left(P_{XFj}^{pq} + P_{YFj}^{pq} + P_{ZFj}^{pq} + P_{SRj}^{pq} + P_0\right) \times t_{AFj}^{pq} \tag{7}$$

where P_{XFj}^{pq}, P_{YFj}^{pq} and P_{ZFj}^{pq} are feeding power of the three axes (normal feeding). The models for P_{XFj}^{pq}, P_{YFj}^{pq} and P_{ZFj}^{pq} are similar. For instance, following Lv et al. [33], P_{XFj}^{pq} can be expressed as:

$$P_{XFj}^{pq} = A_{XF} \times (v_{XFj}^{pq})^2 + B_{XF} \times v_{XFj}^{pq} \tag{8}$$

where coefficients A_{XF} and B_{XF} can be obtained by quadratic regression based on experiment data. The feeding speed at the *X*-axis in the *j*-th feeding activity (v_{XFj}^{pq}) can be calculated by:

$$v_{XFj}^{pq} = v_j^{pq} \times \frac{\Delta X_j^{pq}}{\sqrt{\left(\Delta X_j^{pq}\right)^2 + \left(\Delta Y_j^{pq}\right)^2 + \left(\Delta Z_j^{pq}\right)^2}} \tag{9}$$

where v_j^{pq} is the feeding speed in the *j*-th feeding activity that $v_j^{pq} = n_{SRj}^{pq} \times f_j^{pq}$, where f_j^{pq} is the feed rate [mm/r]. In this scenario, the feeding time of all axes, spindle rotation time and standby time are the same, which is the axial feeding time t_{AFj}^{pq}, $t_{AFj}^{pq} = \frac{\sqrt{\left(\Delta X_j^{pq}\right)^2 + \left(\Delta Y_j^{pq}\right)^2 + \left(\Delta Z_j^{pq}\right)^2}}{n_{SRj}^{pq} \times f_j^{pq}}$.

3.2. Modelling tool change energy consumption

The energy consumption of tool change is affected by the tool change time and tool change power [34]. The tool change power is the sum of standby power and power of tool changer [16]. Thus, the tool change energy consumption portion of the EFT between processing the features F_p and F_q ($E_{TC}^{(F_p,F_q)}$) can be expressed as:

$$E_{TC}^{(F_p,F_q)} = \left(P_0 + P_{TC}^{pq}\right) \times T_{TC}^{(F_p,F_q)}. \tag{10}$$

The time consumed for changing tools is $T_{TC}^{(F_p,F_q)}$, and P_{TC}^{pq} is the corresponding power level of the tool changer. The values of them depend on the number of tool stations rotated for changing tools [35].

In the next section, two solution algorithms and how they have been modified for searching the optimal PSFP are presented.

4. Solution algorithms

Depth-first search and genetic algorithm are applied to search for the optimal PSFP. Depth-first search is selected as one of the solutions because it is able to find the global optimal solution accu-

rately. Comparatively, genetic algorithm normally consumes less time to reach the optimal or near-optimal solution, however, finding out the global optimum is not guaranteed. Hence, experiments are delivered in Section 5 to compare the performance of the two algorithms in solving the aforementioned problem in terms of the solution quality and computation time.

4.1. Depth-first search

Depth-first search (DFS) is an enumeration searching method using the tree traversal technique, which visits the current path as far as possible before backtracking and trying the alternative path in the search tree [36]. The computation time consumed by DFS can be effectively reduced by a pruning approach to avoid the unnecessary path visit. A flowchart of typical DFS is shown in **Fig. 3**. At the beginning of the algorithm, a search tree that can cover all possible paths is generated and a feasible path is randomly selected as the initial upper bound. The nodes of the search tree are visited according to the depth-first searching strategy [37]. If the visited node is not eligible, the algorithm prunes and backtracks to the previous node. If the visited node is eligible and it is the end node, the upper bound will be updated. Then, the algorithm prunes and backtracks to the previous node. If the visited node is eligible but it is not the end node, the algorithm continues to visit the next node. After pruning and backtracking, the algorithm will check whether the stopping conditions have been met or not. If the stopping conditions are met, the latest upper bound will be reported, and the algorithm stops; otherwise, the next node will be visited. The stopping conditions can be that all nodes of the search tree have been visited.

Fig. 3. A flowchart of depth-first search.

4.1.1. Search tree generation for the EFT model

At the beginning of the algorithm, a search tree that can cover all possible PSFPs is generated. For an n-feature part, a search tree with $n + 2$ levels is generated. In the search tree, a node denotes a feature and the level denotes the position in the sequence. Therefore, a node at the k-th level of the search tree indicates a feature at the k-th position of the sequence. The root node at the 1-st level and the node at the $n + 2$-th level represent the virtual first and final features F_0 and F_{n+1}, respectively. A complete path in the search tree represents a possible PSFP. Considering a 3-feature part, a search tree with 5 levels is generated. A complete path labelled by bold blue lines in the search tree represents a possible PSFP F_0-F_1-F_3-F_2-F_4, as shown in **Fig. 4**.

Fig. 4. The search tree for a 3-feature part.

4.1.2. Conditions of an eligible node and pruning

An eligible node meets the following three conditions: (1) The node has not been visited in the current path. (2) The node satisfies all of the precedence constraints. (3) The current path value is smaller than the upper bound after visiting the current node. The current path value is the sum from the root node to the current node. The corresponding nodes will be pruned if any condition above is not met, as illustrated in **Fig. 4**.

4.2. Genetic algorithm

Genetic algorithm (GA) is a heuristic search technique, which imitates the process of natural evolution by combining the survival of the fittest to create offspring [38]. The offspring replaces weak solutions in each generation and finally the optimal or near-optimal solutions to the optimisation problem are generated [28]. A flowchart of standard GA is shown in **Fig. 5**. At the beginning of the algorithm, an initial population with a size of N chromosomes is randomly generated as the first generation. In the following generations, chromosomes are selected to breed a new generation through a fitness-based process measured by a fitness function [39]. The fitness function is defined as the genetic representation and measures the quality of each chromosome in the population [40]. The chromosomes with a higher fitness have more probabilities to be selected. The next generation of chromosomes are generated from these selected chromosomes through the GA operators of (1) Crossover: an exchange of segments between the chromosomes and (2) Mutation: a random modification on the chromosome [28]. This generational process is repeated until a stopping condition has been met [41]. The stopping condition can be the specified maximum number of generations reached.

Fig. 5. A flowchart of genetic algorithm.

4.2.1. Encoding scheme and fitness evaluation

In this research, a PSFP is encoded to a chromosome by integer coding [42]. Each gene in the chromosome corresponds to a specific feature. For example, a PSFP F_0-F_5-F_7-F_3-F_6-F_1-F_4-F_2-F_8 can be encoded as a chromosome [057361428]. The gene 3 represents the feature F_3. If the gene sequence of a chromosome violates the precedence constraints between features, the corresponding chromosome can be corrected by exchanging and adjusting the positions of illegal genes in the sequence. The fitness of each chromosome is evaluated by a fitness function which is the reciprocal of the total EFT for a PSFP that $Fitness = \frac{1}{E_{FS}} = \frac{1}{\sum_{k=1}^{n+1} E_{FT}^{(S_k, S_{k+1})}}$.

4.2.2. Selection, crossover and mutation operators

The selection operator aims at selecting the chromosomes in the current generation to reproduce offspring. The proportional roulette wheel selection is used for this research. More details of this selection operator can be referred to Razali and Geraghty [43].

The partially mapped crossover (PMX) is adopted as the crossover operator [44]. For instance, given parents $B_1 = [057361428]$ and $B_2 = [043652178]$, PMX generates children B_1' and B_2' by the following procedures.

Two points are randomly chosen as the crossover points according to the length of the chromosome, and then the segments between the two points of B_1 and B_2 are exchanged to generate two new chromosomes C_1 and C_2, as below:

$$\begin{matrix} B_1 = [057|3614|28] \\ B_2 = [043|6521|78] \end{matrix} \overset{\text{Crossover}}{\Longrightarrow} \begin{matrix} C_1 = [057|6521|28] \\ C_2 = [043|3614|78] \end{matrix}.$$

After the above operation, there are probably some genes repeated in the new chromosomes. To correct this, the repeated genes outside segments between the crossover points are replaced according to the partially mapped method. For example, genes at the 2-nd loci and the 5-th loci are repeated and genes at the 6-th loci and the 8-th loci are repeated in the chromosome C_1. The 2-nd loci and the 8-th loci are at the outside of segments between the crossover points. Thus, the genes at the 2-nd and the 8-th loci are replaced by the gene 3 and the gene 4, respectively. Finally, the two child chromosomes are obtained as:

$$\begin{matrix} B_1' = [037652148] \\ B_2' = [052361478] \end{matrix}.$$

The swap mutation is adopted as the mutation operator which means two arbitrary genes of a chromosome are selected and swap the values [45]. Following the above example, B_1'' is the final child chromosome of B_1 after applying a mutation on B_1' as:

$$B_1' = [03\boxed{7}652\boxed{1}48] \overset{\text{Mutation}}{\Longrightarrow} B_1'' = [03\boxed{1}652\boxed{7}48].$$

5. Case study

A prismatic part named part A with 15 actual features is used as the case study. Within the background of this research, 17 features are considered for this case, which are F_1 (plain), F_2 (stair), F_3 (groove), F_4 (depression), F_5 (notch), F_6 (notch), F_7 (hole), F_8 (hole), F_9 (hole), F_{10} (hole), F_{11} (hole), F_{12} (hole), F_{13} (hole), F_{14} (hole) and F_{15} (hole) and 2 virtual features F_0 and F_{16}, as shown in **Fig. 6**. The feature F_1 is required to be machined prior to any other features ($S_2 = F_1$). A machining centre (XHF-714F) is employed as the processor for part A. The experiment set-up for power data collection of XHF-714F is the same as that in Hu et al. [17]. The relationships between the number of tool stations rotated, power of tool changer and tool change time of XHF-714F are listed in **Table 1**. Standby power and axial rapid feeding power are shown in **Table 2**. All the data in the aforementioned two tables are obtained by experiment measurement. Coefficients which are obtained by regression based on experiment data for models of spindle rotation power and axial feeding power are listed in **Table 3**. The speed of axial rapid feeding is obtained from the manual of XHF-714F, as shown in **Table 4**. Besides, each tool station and its corresponding cutter, and each cutter's corresponding features are presented in **Table 5**. Tool station #1 is used as the start in the experiment. The origin of coordinates *O* (0, 0, 0) is located at the centre of top surface of the part's blank. Coordinate point *G* (-80, -80, 60) is used as the start and end position of the tool, and the position for tool change.

Fig. 6. A prismatic part with 15 actual features and 2 virtual features.

Table 1 The relationships between the number of tool stations rotated, power of tool changer and tool change time of XHF-714F.

Table 2 Standby power and axial rapid feeding power of XHF-714F.

Table 3 Coefficients in power models of XHF-714F.

Table 4 Axial rapid feeding speed of XHF-714F.

Table 5 Relationships between the tool station number, cutters and features.

To prove the effectiveness of the proposed optimisation approaches in reducing the EFT, the following comparison is conducted. A PSFP produced by the classical sequencing technique Left-to-Right (LTR) [22] serves as the benchmark to represent the existing approach to arranging the PSFP without the energy-saving consideration. The benchmark PSFP generated by LTR is $F_0 - F_1 - F_2 - F_4 - F_{12} - F_{13} - F_7 - F_8 - F_3 - F_{11} - F_{10} - F_9 - F_5 - F_6 - F_{15} - F_{14} - F_{16}$. The aforementioned depth-first

search (DFS) and genetic algorithm (GA) used in this research are developed on Dev C++ 5.11.0 software with the programming language C++. The parameters of the computation facility used for experiments are as follows: Intel (R) Core (TM) i7-2630 QM CPU with 2.00 GHz frequency; 4.00 GB RAM; Windows 7 (64bit) operating system.

For this 17 features part, considering the two virtual features are fixed as the first and final ones on the feature sequence ($S_1 = F_0$, $S_{17} = F_{16}$), there are 256 possible pairs of features. In the following, the value calculation procedure for the EFT between processing F_2 and F_5 ($E_{FT}^{(F_2,F_5)}$) is used as example to show how to use the models in Section 3.

Based on above and Expression (1), $E_{FT}^{(F_2,F_5)}$ is expressed as:

$$E_{FT}^{(F_2,F_5)} = E_{TP}^{(F_2,F_5)} + E_{TC}^{(F_2,F_5)}$$

where $E_{TP}^{(F_2,F_5)}$ and $E_{TC}^{(F_2,F_5)}$ are energy consumption of tool path and tool change, respectively, during the feature transition from the feature F_2 to its post-feature F_5, which are calculated as follows.

(1) Calculation of $E_{TP}^{(F_2,F_5)}$

As shown in **Fig. 6**, there are five feeding activities in the feature transition from F_2 to F_5. The process parameters of them are listed in **Table 6**. According to Expression (3), $E_{TP}^{(F_2,F_5)}$ is calculated by:

$$E_{TP}^{(F_2,F_5)} = \sum_{j=1}^{5} A_j^{(F_2,F_5)}$$

where $A_1^{(F_2,F_5)}$,…, $A_5^{(F_2,F_5)}$ are energy consumption of the first to the fifth feeding activity, respectively. Here the calculation of $A_1^{(F_2,F_5)}$ is used as an example.

Table 6 Process parameters of five feeding activities in the feature transition.

Normal feeding is used for the first feeding activity. Thus, Expression (7) is employed to calculate its energy consumption as:

$$A_1^{(F_2,F_5)} = (P_{XF1}^{25} + P_{YF1}^{25} + P_{ZF1}^{25} + P_{SR1}^{25} + P_0) \times t_{AF1}^{25}.$$

According to Equations (9) and parameters in **Table 6**, the values of feeding speed at *X*-axis, *Y*-axis and *Z*-axis in the first feeding activity are:

$$v_{XF1}^{25} = 2200 \times 0.2 \times \frac{|-37-(-37)|}{\sqrt{|-37-(-37)|^2+|40-30|^2+|-15-(-15)|^2}} = 0\text{mm/min},$$

$$v_{YF1}^{25} = 2200 \times 0.2 \times \frac{|40-30|}{\sqrt{|-37-(-37)|^2+|40-30|^2+|-15-(-15)|^2}} = 440\text{mm/min},$$

$$v_{ZF1}^{25} = 2200 \times 0.2 \times \frac{|-15-(-15)|}{\sqrt{|-37-(-37)|^2+|40-30|^2+|-15-(-15)|^2}} = 0\text{mm/min}.$$

Then according to Equation (8) and coefficients in **Table 3**, the values of feeding power of all axes are:

$$P_{XF1}^{25} = 5 \times 10^{-7} \times 0^2 + 0.049 \times 0 = 0\text{W},$$

$$P_{YF1}^{25} = -1 \times 10^{-6} \times 440^2 + 0.043 \times 440 = 18.73\text{W},$$

$$P_{ZF1}^{25} = -1 \times 10^{-7} \times 0^2 + 0.0461 \times 0 = 0\text{W}.$$

According to Equation (6) and coefficients in **Table 3**, spindle rotation power is:

$$P_{SR1}^{25} = 0.086 \times 2200 + 14.76 = 203.96\text{W}.$$

Standby power is: $P_0 = 371.0\text{W}$.

Axial feeding time for the first feeding activity is:

$$t_{AF1}^{25} = \frac{60 \times \sqrt{(-37-(-37))^2+(40-30)^2+(-15-(-15))^2}}{2200 \times 0.2} = 1.364\text{s}.$$

Based on above, energy consumption of the first feeding activity in the feature transition from F_2 to F_5 is:

$$A_1^{(F_2,F_5)} = (0 + 18.73 + 0 + 203.96 + 371.0) \times 1.364 = 809.57\text{J}.$$

Similarly, energy consumption of other four feeding activities can be calculated as: $A_2^{(F_2,F_5)} = 185.11\text{J}$, $A_3^{(F_2,F_5)} = 1029.64\text{J}$, $A_4^{(F_2,F_5)} = 1321.25\text{J}$, and $A_5^{(F_2,F_5)} = 242.87\text{J}$.

By summing up energy consumption of the five feeding activities, the value of $E_{TP}^{(F_2,F_5)}$ is:

$$E_{TP}^{(F_2,F_5)} = 3588.45\text{J}.$$

(2) Calculation of $E_{TC}^{(F_2,F_5)}$

According to Expression (10), $E_{TC}^{(F_2,F_5)}$ is calculated by:

$$E_{TC}^{(F_2,F_5)} = (P_0 + P_{TC}^{25}) \times T_{TC}^{(F_2,F_5)}.$$

According to **Table 5**, the corresponding cutters for F_2 and F_5 locate at tool station #1 and #2, respectively. Thus, one interval of the tool station rotation is required. According to **Table 1**, power of the tool changer is: $P_{TC}^{25} = 84.8\text{W}$, and tool change time is: $T_{TC}^{(F_2,F_5)} = 17.6\text{s}$. Therefore, $E_{TC}^{(F_2,F_5)} = (371.0 + 84.8) \times 17.6 = 8022.08\text{J}$. By summing up $E_{TP}^{(F_2,F_5)}$ and $E_{TC}^{(F_2,F_5)}$, the EFT from F_2 to F_5 is calculated as: $E_{FT}^{(F_2,F_5)} = 3588.45 + 8022.08 = 11610.5\text{J}$. The value of $E_{FT}^{(F_2,F_5)}$ and other 255 EFT values are listed in **Table 7**.

Table 7 Energy consumption of feature transitions between features in the part.

Based on the data in **Table 7**, the EFT for the benchmark PSFP is 145894.3J. Comparatively, the developed DFS achieves the global optimum of the minimum EFT, which is 104162.7J, with computation time of 42.13 seconds. The corresponding PSFP is $F_0-F_1-F_2-F_5-F_6-F_3-F_4-F_8-F_9-F_{10}-F_7-F_{12}-F_{13}-F_{14}-F_{15}-F_{11}-F_{16}$. The searching process of DFS is presented in **Fig. 7**. Therefore, 28.60% [(145894.3-104162.7)/145894.3] EFT can be reduced by using DFS compared to LTR technique.

The parameter values used in GA are obtained by tuning, and their values are as follows: population size= 100, crossover probability= 0.9, mutation probability= 0.05, and generation= 300. By running GA for several times, it can also achieve the global minimum EFT (104162.7J) with computation time of 2.42 seconds. The corresponding PSFP is the same as that produced by DFS. A searching process of GA for the optimal solution is shown in **Fig. 8**. However, in most of the runs of GA, it can only achieve the near-optimal solutions for this case. For example, a near-minimum EFT that GA can get is 104179.8 J. The corresponding PSFP is $F_0-F_1-F_2-F_4-F_3-F_6-F_5-F_{10}-F_9-F_8-F_7-F_{15}-F_{14}-F_{13}-F_{12}-F_{11}-F_{16}$. It also consumes less computation time (2.48 seconds) to get the near-optimal solution. A searching process of GA for a near-optimal solution of this case is shown in **Fig. 9**.

Fig. 7. The searching process of depth-first search for the optimal solution.

Fig. 8. A searching process of genetic algorithm for the optimal solution.

Fig. 9. A searching process of genetic algorithm for a near-optimal solution.

According to the optimisation results, for this case, GA usually returns a near-optimal solution while DFS always obtains the global optimum. Thus, compared to GA, DFS is superior in finding the most energy-saving PSFP. Although the solution quality of GA is probably little inferior to that of DFS, its computation time is about 94.11% [(42.13-2.48)/42.13] lesser than that of DFS. Moreover, when the number of features in a part is increasing, the computation time of DFS probably increases sharply and becomes intolerable. In this situation, GA is preferable to be employed to get the near-optimal PSFP within reasonable computation time.

6. Discussion

The case study has shown that 28.60% of the EFT can be reduced by using the single objective optimisation, which validates the effectiveness of our approach in single machine environment. However, in the real manufacturing circumstance, a part usually requires more than one machine tool to finish all of the processing. Thus, the performance of our approach on the EFT reduction in multi-machine environment is discussed and validated in this section. In addition, it is not reasonable to only reduce the EFT without considering other objectives including the machining time, quality and cost, which can cause machine tool tardiness and product quality problems. Thus, a multi-objective model considering the EFT is developed, and then the effect of the EFT minimisation on other objectives is demonstrated and discussed.

6.1. EFT reduction in multi-machine environment

If a part requires more than one machine tool, its features to be processed on the same machine can be sorted and sequenced to reduce the EFT. For example, it is assumed that the part A in **Fig. 6** requires two machine tools including a CNC milling machine and a CNC drilling machine to finish all of its features. Specifically, a CNC milling machine is employed to process the features including F_1 (plain), F_2 (stair), F_3 (groove), F_4 (depression), F_5 (notch) and F_6 (notch); a CNC drilling machine is employed to process the other features including F_7 (hole), F_8 (hole), F_9 (hole), F_{10} (hole), F_{11} (hole), F_{12} (hole), F_{13} (hole), F_{14} (hole) and F_{15} (hole).

Two benchmark PSFPs generated by the LTR technique for the CNC milling machine and the CNC drilling machine are $F_0-F_1-F_2-F_4-F_3-F_5-F_6-F_{16}$ and $F_0-F_{12}-F_{13}-F_7-F_8-F_{11}-F_{10}-F_9-F_{15}-F_{14}-F_{16}$. It is assumed that the parameters of two machine tools are the same as that of XHF-714F, thus the data in bold font in **Table 7** can be utilised for the EFT calculation. Then, the EFT for the two benchmark PSFPs is 20918.2J and 105335.9J, respectively. In total, the benchmark EFT for part A is 126254.1J (20918.2+105335.9) in two-machine environment. Comparatively, the optimal PSFPs generated by DFS for the two machine tools are $F_0-F_1-F_2-F_5-F_6-F_3-F_4-F_{16}$ and $F_0-F_7-F_8-F_9-F_{10}-F_{15}-F_{14}-F_{13}-F_{12}-F_{11}-F_{16}$. According to data in **Table 7**, the EFT for the two optimal PSFPs is 20774.9J and 84132.3J, respectively. In total, the minimum EFT for part A is 104907.2J (20774.9+84132.3) in two-machine environment. Consequently, when part A requires two machine tools, our approach still achieves a 16.91% [(126254.1-104907.2)/126254.1] EFT reduction, which validates its effectiveness in multi-machine environment.

6.2. Multi-objective model considering the EFT

The developed single objective model for minimising the EFT can integrate with the models for optimising other objectives such as the machining time, quality and cost to obtain the required multi-objective model. For example, to avoid machine tool tardiness, the time consumption of feature transitions (TFT) is regarded as a new objective and integrated with the developed EFT model to obtain a bi-objective model for balancing the TFT and the EFT. Based on Expression (2), the bi-objective model is developed as:

$$\begin{cases} minimise\ E_{FS} = \sum_{k=1}^{n+1} E_{FT}^{(S_k,S_{k+1})} \\ minimise\ T_{FS} = \sum_{k=1}^{n+1} T_{FT}^{(S_k,S_{k+1})} \end{cases} \tag{11}$$

where T_{FS} is the total TFT based on a specific PSFP, and $T_{FT}^{(S_k,S_{k+1})}$ is the TFT between processing the feature at the k-th position and the feature at the $k+1$-th position of a sequence. It is assumed that the features F_p and F_q are located at the k-th position and the $k+1$-th position of a sequence, respectively. Then, by referring to Expression (1), $T_{FT}^{(S_k,S_{k+1})}$ can be expressed as:

$$T_{FT}^{(S_k,S_{k+1})} = T_{FT}^{(F_p,F_q)} = T_{TP}^{(F_p,F_q)} + T_{TC}^{(F_p,F_q)} \tag{12}$$

where $T_{TP}^{(F_p,F_q)}$ is time consumption of tool path in the feature transition from the feature F_p to its post-feature F_q. By referring to Expression (3), $T_{TP}^{(F_p,F_q)}$ is expressed as:

$$T_{TP}^{(F_p,F_q)} = \sum_{j=1}^{m} B_j^{(F_p,F_q)} \quad (13)$$

where $B_j^{(F_p,F_q)}$ is time consumption of the j-th feeding activity in the feature transition from F_p to F_q. In a rapid feeding activity, $B_j^{(F_p,F_q)}$ equals to t_{ARj}^{pq}; otherwise, it equals to t_{AFj}^{pq}.

After obtaining the above bi-objective model, multi-objective optimisation approaches such as Non-dominated Sorting Genetic Algorithm II (NSAG-II) and Strength Pareto Evolutionary Algorithm (SPEA) can be employed to find a set of optimal PSFPs that result in the optimal trade-offs between TFT and EFT [46]. These optimisation approaches will be researched in the future. In the following, the effect of the EFT minimisation on the TFT is demonstrated and discussed based on the developed TFT model.

According to Expressions (11)-(13) and data in **Tables 1**, **4**, **5** and **6**, the TFT based on the optimal PSFP which results in the EFT minimisation of part A is calculated as follows:

$$T_{FS}\,(\text{EFT minimisation}) = T_{FT}^{(F_0,F_1)} + T_{FT}^{(F_1,F_2)} + T_{FT}^{(F_2,F_5)} + T_{FT}^{(F_5,F_6)} + T_{FT}^{(F_6,F_3)} + T_{FT}^{(F_3,F_4)} + T_{FT}^{(F_4,F_8)} + T_{FT}^{(F_8,F_9)} + T_{FT}^{(F_9,F_{10})} + T_{FT}^{(F_{10},F_7)} + T_{FT}^{(F_7,F_{12})} + T_{FT}^{(F_{12},F_{13})} + T_{FT}^{(F_{13},F_{14})} + T_{FT}^{(F_{14},F_{15})} + T_{FT}^{(F_{15},F_{11})} + T_{FT}^{(F_{11},F_{16})} = 0.613 + 1.803 + 20.828 + 2.277 + 3.227 + 1.021 + 32.486 + 12.875 + 12.875 + 12.875 + 30.850 + 12.922 + 13.222 + 12.922 + 33.872 + 0.640 = 205.31\text{s}.$$

In comparison, a PSFP without considering the EFT reduction for part A is generated by the LTR technique, and the TFT based on this PSFP is: $T_{FS}\,(\text{LTR technique}) = 284.94s$. Thus, 27.95% [(284.94-205.31)/284.94] of the TFT reduction benefits from the EFT minimisation in the multi-objective problem. However, the EFT minimisation is not always beneficial to the TFT reduction. For example, when a PSFP with the minimum TFT is adjusted to a PSFP with the minimum EFT, its TFT can increase. In this situation, the trade-off between the minimisation of TFT and EFT should be made.

7. Conclusions and future work

Reducing the electricity consumption of machine tools during the run-time operations gains more and more importance in modern manufacturing. The model for the single objective optimisation problem which aims at minimising the energy consumption of feature transitions (EFT) has been introduced. The model was developed by understanding and characterising the energy consumption

of machine tools while executing the rapid and normal feeding activities and the tool change. The total amount of the EFT for processing a part on a single machine can vary by modifying the processing sequence of features of the part (PSFP). To find the optimal PSFP which results in the minimisation of the total EFT, depth-first search and genetic algorithm are employed as the optimisation approaches.

In the case study, the optimal and near-optimal sequences of features for a 15 features part which is processed by a machining centre (XHF-714F) have been found. The optimal PSFP achieves a 28.60% EFT reduction. This validates the effectiveness of the developed mathematic model and optimisation approaches in single machine environment. When the part requires more than one machine tool to finish all of its features, this approach still achieves a 16.91% EFT reduction. Finally, the developed EFT model is integrated with a TFT model to obtain a bi-objective model for balancing the TFT and the EFT. A case shows that 27.95% of the TFT reduction benefits from the EFT minimisation.

In this research, it is time-consuming and error-prone to process the data of machine tools and parts for the EFT model and then calculate the EFT values between each pair of features. Thus, the automation for the EFT calculation can be improved. One limitation of this research is that the energy consumption of machine tools during setup change and machine change has not been considered as a portion of the EFT. For the next step, research on reducing the energy consumed for setup change and machine change by adjusting the PSFP will be conducted. Besides, multi-objective optimisation approaches will be employed to obtain the optimal PSFPs that result in the optimal trade-offs among the machining energy consumption, time, quality, cost and other objectives. Finally, the proposed feature sequencing approach will be combined with the existing cutting parameter optimisation to promote the energy-aware integrated process planning for machining.

Acknowledgments

The authors would like to thank the support from the National Natural Science Foundation of China (Grant No.U1501248), the Nantaihu Innovation Program of Huzhou Zhejiang China, the China Scholarship Council (Grant No. 201406320033), the EPSRC Centre for Innovative Manufacturing in Industrial Sustainability (Grant No. EP/I033351/1), and the EPSRC EXHUME Project (Efficient X-sector use of HeterogeneoUs MatErials in Manufacturing) (Grant No. EP/K026348/1).

1 References

[1] Wang Y, Li L. Time-of-use based electricity demand response for sustainable manufacturing systems. Energy 2013; 63: 233-44.

[2] Cai W, Liu F, Zhang H, Liu P, Tuo J. Development of dynamic energy benchmark for mass production in machining systems for energy management and energy-efficiency improvement. Appl Energ 2017; 202: 715-25.

[3] Newman ST, Nassehi A, Imani-Asrai R, Dhokia V. Energy efficient process planning for CNC machining. CIRP J Manuf Sci Technol 2012; 5(2): 127-36.

[4] Hu L, Peng T, Peng C, Tang R. Energy consumption monitoring for the order fulfilment in a ubiquitous manufacturing environment. Int J Adv Manuf Tech 2017; 89(9-12):3087-100.

[5] EIA. Annual energy review; 2011. Retrieved from,
http://www.eia.gov/totalenergy/data/annual/index.cfm. Last visited: 27/6/2017.

[6] Schudeleit T, Züst S, Weiss L, Wegener K. The total energy efficiency index for machine tools. Energy 2016; 102: 682-93.

[7] Zhou L, Li J, Li F, Meng Q, Li J, Xu X. Energy consumption model and energy efficiency of machine tools: a comprehensive literature review. J Clean Prod 2016; 112: 3721-34.

[8] Dahmus JB, Gutowski TG. An environmental analysis of machining. In: ASME 2004 International Machining Engineering Congress and RD&D Expo; 2004. p. 643-52.

[9] Kordonowy DN. A power assessment of machining tools [dissertation]. Massachusetts Institute of Technology; 2002.

[10] Liu Y, Dong HB, Lohse N, Petrovic S. Reducing environmental impact of production during a Rolling Blackout policy – A multi-objective schedule optimisation approach. J Clean Prod 2015; 102: 418-27.

[11] Cai W, Liu F, Zhou X, Xie J. Fine energy consumption allowance of workpieces in the mechanical manufacturing industry. Energy 2016; 114: 623-33.

[12] Lv JX. Research on energy supply modeling of computer numerical control machine tools for low carbon manufacturing [dissertation]. Zhejiang University; 2014 [in Chinese].

[13] Cai W, Liu F, Xie J, Liu P, Tuo J. A tool for assessing the energy demand and efficiency of machining systems: Energy benchmarking. Energy 2017; 138: 332-47.

[14] Sheng P, Srinivasan M, Kobayashi S. Multi-objective process planning in environmentally conscious manufacturing: a feature-based approach. CIRP Ann-Manuf Technol 1995; 44(1):433-7.

[15] Li W, Zein A, Kara S, Herrmann C. An investigation into fixed energy consumption of machine tools. In: Glocalized Solutions for Sustainability in Manufacturing; 2011. p. 268-73.

[16] Jia S. Research on energy demand modeling and intelligent computing of machining process for low carbon manufacturing [dissertation]. Zhejiang University; 2014 [in Chinese].

[17] Hu L, Peng C, Evans S, Peng T, Liu Y, Tang R, Tiwari A. Minimising the machining energy consumption of a machine tool by sequencing the features of a part. Energy 2017; 121:292-305.

[18] Yin R, Cao H, Li H, Sutherland JW. A process planning method for reduced carbon emissions. Int J Comput Integ M 2014; 27(12):1175-86.

[19] Hu L, Tang R, He K, Jia S. Estimating machining-related energy consumption of parts at the design phase based on feature technology. Int J Prod Res 2015; 53(23): 7016-33.

[20] Wiener R. Branch and bound implementations for the traveling salesperson problem - part 1: a solution with nodes containing partial tours with constraints. J Obj Technol 2003; 2(2): 65-86.

[21] Srinivasan M, Sheng P. Feature based process planning in environmentally conscious machining–Part 2: macroplanning. Robot Cim-Int Manuf 1999; 15(3): 271-81.

[22] Al-Sahib NKA, Abdulrazzaq HF. Tool path optimization of drilling sequence in CNC machine using genetic algorithm. Innov Syst Des Eng 2014; 5(1): 15-26.

[23] Abu Qudeiri J, Yamamoto H, Ramli R. Optimization of operation sequence in CNC machine tools using genetic algorithm. J Adv Mech Des Syst 2007; 1(2): 272-82.

[24] Onwubolu GC, Clerc M. Optimal path for automated drilling operations by a new heuristic approach using particle swarm optimization. Int J Prod Res 2004; 42(3): 473-91.

[25] Kolahan F, Liang M. Optimization of hole-making operations: a tabu-search approach. Int J Mach Tool Manu 2000; 40(12): 1735-53.

[26] Ghaiebi H, Solimanpur M. An ant algorithm for optimization of hole-making operations. Comput Ind Eng 2007; 52(2): 308-19.

[27] Singh S, Deb S. An intelligent methodology for optimising machining operation sequence by ant system algorithm. Int J Ind Syst Eng 2014; 16(4):451-71.

[28] Bhaskara Reddy SV. Operation sequencing in CAPP using genetic algorithms. Int J Prod Res 1999; 37(5): 1063-74.

[29] Lee DH, Kiritsis D, Xirouchakis P. Branch and fathoming algorithms for operation sequencing in process planning. Int J Prod Res 2001; 39(8): 1649-69.

[30] Lee DH, Kiritsis D, Xirouchakis P. Search heuristics for operation sequencing in process planning. Int J Prod Res 2001; 39(16): 3771-88.

[31] Zhao GY, Liu ZY, He Y, Cao HJ, Guo YB. Energy consumption in machining: Classification, prediction, and reduction strategy. Energy 2017; 133: 142-57.

[32] Zhong Q, Tang R, Lv J, Jia S, Jin M. Evaluation on models of calculating energy consumption in metal cutting processes: a case of external turning process. Int J Adv Manuf Technol 2016; 82(9): 2087-99.

[33] Lv J, Tang R, Jia S. Therblig-based energy supply modeling of computer numerical control machine tools. J Clean Prod 2014; 65: 168-77.

[34] He Y, Liu F, Wu T, Zhong FP, Peng B. Analysis and estimation of energy consumption for numerical control machining. P I Mech Eng B-J Eng 2012; 226: 255-66.

[35] Gara S, Bouzid W, Amar MB, Hbaieb M. Cost and time calculation in rough NC turning. Int J Adv Manuf Technol 2009; 40(9-10): 971-81.

[36] Rathi G, Goel S. Applications of depth first search: a survey. Int J Eng Res Technol 2013; 2(7): 1341-7.

[37] Bhattacharya S, Roy R, Bhattacharya S. An exact depth-first algorithm for the pallet loading problem. Eur J Oper Res 1998; 110(3): 610-25.

[38] Chu PC, Beasley JE. A genetic algorithm for the multidimensional knapsack problem. J Heuristics 1998; 4(1): 63-86.

[39] Bajpai P, Kumar M. Genetic algorithm–an approach to solve global optimization problems. Indian J Comput Sci Eng 2010; 1(3): 199-206.

[40] Reddy RR, Vali SM, Varma PD. Reduction of side lobe levels of sum patterns from discrete arrays using genetic algorithm. Int J Eng Res Appl 2013; 3(4): 1312-7.

[41] Ruiz R, Maroto C, Alcaraz J. Two new robust genetic algorithms for the flowshop scheduling problem. Omega 2006; 34(5): 461-76.

[42] Forrest S. Genetic algorithms: principles of natural selection applied to computation. Science 1993; 261(5123): 872-8.

[43] Razali NM, Geraghty J. Genetic algorithm performance with different selection strategies in solving TSP. In: Proceedings of the world congress on engineering 2011(WCE); 2011. p. 1134-9.

[44] Goldberg DE, Lingle R. Alleles, loci, and the traveling salesman problem. In: Proceedings of the First International Conference on Genetic Algorithms and Their Applications; 1985. p.154-9.

[45] Liu Y, Dong H, Lohse N, Petrovic S, Gindy N. An investigation into minimising total energy consumption and total weighted tardiness in job shops. J Clean Prod 2014; 65: 87-96.

[46] Deb K, Pratap A, Agarwal S, Meyarivan TAMT. A fast and elitist multiobjective genetic algorithm: NSGA-II. IEEE T Evolut Comput 2002; 6(2): 182-97.

Table 1 The relationships between the number of tool stations rotated, power of tool changer and tool change time of XHF-714F.

	The number of tool stations rotated								
	0	1	2	3	4	5	6	7	8
Power [W]	0.0	84.8	90.4	93.6	96.2	100.1	100	104.2	102.4
Time [s]	0.0	17.6	19.0	20.0	20.9	21.9	23.5	24.1	25.3

Table 2 Standby power and axial rapid feeding power of XHF-714F.

Item	Power [W]
Standby power P_0	371.0
X-axial rapid feeding power P_{XR}	855.8
Y-axial rapid feeding power P_{YR}	504.9
Z-axial upward and downward rapid feeding power (P_{ZR}^{U}, P_{ZR}^{D})	(659.1, 573.4)

Table 3 Coefficients in power models of XHF-714F.

Item	Coefficient
Monomial coefficient and constant in the spindle rotation power model (B_{SR}, C_{SR})	(0.086, 14.76)
Quadratic coefficient in the feeding power model of *X*-axis, *Y*-axis, *Z*-axis upward and downward (A_{XF}, A_{YF}, A_{ZF}^{U}, A_{ZF}^{D})	(5×10^{-7}, -1×10^{-6}, -5×10^{-7}, -1×10^{-7})
Monomial coefficient in the feeding power model of *X*-axis, *Y*-axis, *Z*-axis upward and downward (B_{XF}, B_{YF}, B_{ZF}^{U}, B_{ZF}^{D})	(0.0491, 0.043, 0.059, 0.0461)

Table 4 Axial rapid feeding speed of XHF-714F.

Item	Speed [m/min]
Rapid feeding speed of *X*-axis, *Y*-axis and *Z*-axis (v_{XR}, v_{YR}, v_{ZR})	(12, 12, 10)

Table 5 Relationships between the tool station number, cutters and features.

	The tool station number of the tool changer				
	#1	#2	#3	#4	#5
Cutters	W400F-FS	W400F-FS	NACHI SD8(8)	NACHI SD8(10)	NACHI SD8(12)
Features	F_1, F_2	F_3, F_4, F_5, F_6	F_7, F_8, F_9, F_{10}	F_{12}, F_{13}, F_{14}, F_{15}	F_{11}

Table 6 Process parameters of five feeding activities in the feature transition.

The j-th feeding activity	Feeding method	Start coordinate position	End coordinate position	Spindle speed n_{SRj}^{25} [rpm]	Feed rate f_j^{25} [mm/r]
1	Normal	(-37, 30, -15)	(-37, 40, -15)	2200	0.2
2	Rapid	(-37, 40, -15)	(-37, 40, 10)	2200	-
3	Rapid	(-37, 40, 10)	(-80, -80, 60)	2200	-
4	Rapid	(-80, -80, 60)	(61, -40, -1.5)	2200	-
5	Normal	(61, -40, -1.5)	(61, -37, -1.5)	2200	0.2

Table 7 Energy consumption of feature transitions between features in the part.

Energy [J]	F_1	F_2	F_3	F_4	F_5	F_6	F_7	F_8	F_9	F_{10}	F_{11}	F_{12}	F_{13}	F_{14}	F_{15}	F_{16}
F_0	**775.2**	**852.3**	**9780.0**	**8954.2**	**9586.2**	**9827.8**	**14955.7**	**15162.2**	**15354.8**	**15241.2**	**17111.3**	**15369.7**	**15558.2**	**16051.7**	**15950.7**	∞
F_1	∞	**1582.6**	**11602.7**	**10776.9**	**11408.9**	**11650.5**	16778.4	16984.9	17177.5	17063.9	18934.0	17192.4	17380.9	17874.4	17773.4	**1822.7**
F_2	**1534.6**	∞	**11804.4**	**10978.5**	**11610.5**	**11852.2**	16980.0	17186.6	17379.1	17265.5	19135.7	17394.1	17582.5	18076.0	17975.0	**2024.3**
F_3	**10031.8**	**10109.0**	∞	**1090.1**	**1007.5**	**967.2**	15445.7	15652.2	15844.8	15731.2	17873.4	16078.9	16267.3	16760.8	16659.8	**1234.5**
F_4	**10492.6**	**10569.8**	**2392.8**	∞	**2440.6**	**2425.4**	15906.5	16113.0	16305.6	16192.0	18334.2	16539.7	16728.1	17221.6	17120.6	**1695.3**
F_5	**11225.9**	**11303.0**	**2354.1**	**2370.0**	∞	**1667.1**	16639.8	16846.3	17038.8	16925.2	19067.4	17272.9	17461.4	17954.9	17853.9	**2428.6**
F_6	**11311.7**	**11388.8**	**2354.1**	**2370.0**	**1667.1**	∞	16725.6	16932.1	17124.7	17011.1	19153.3	17358.7	17547.2	18040.7	17939.7	**2514.4**
F_7	10426.4	10503.6	10664.6	9838.8	10470.8	10712.4	∞	**5871.1**	**6063.7**	**5950.1**	**16998.1**	**14984.4**	**15172.9**	**15666.4**	**15565.4**	**884.6**
F_8	10633.0	10710.1	10871.2	10045.4	10677.4	10919.0	**5871.1**	∞	**5950.1**	**6063.7**	**17204.6**	**15191.0**	**15379.4**	**15872.9**	**15771.9**	**1091.2**
F_9	10825.5	10902.7	11063.7	10237.9	10869.9	11111.5	**6063.7**	**5950.1**	∞	**5871.1**	**17397.2**	**15383.5**	**15572.0**	**16065.5**	**15964.5**	**1283.7**
F_{10}	10711.9	10789.0	10950.1	10124.3	10756.3	10997.9	**5950.1**	**6063.7**	**5871.1**	∞	**17283.6**	**15269.9**	**15458.4**	**15951.9**	**15850.9**	**1170.1**
F_{11}	11714.3	11791.4	12224.6	11398.7	12030.7	12272.4	**16130.3**	**16336.8**	**16529.4**	**16415.8**	∞	**15274.4**	**15462.9**	**15956.4**	**15855.4**	**1174.6**
F_{12}	10919.4	10996.5	11376.8	10550.9	11182.9	11181.7	**15063.4**	**15269.9**	**15462.5**	**15348.9**	**16221.1**	∞	**5926.5**	**6485.6**	**6384.7**	**852.2**
F_{13}	11107.9	11185.0	11565.2	10739.4	11371.4	11613.0	**15251.8**	**15458.4**	**15650.9**	**15537.3**	**16409.6**	**5926.5**	∞	**6384.7**	**6485.6**	**1040.6**
F_{14}	11601.4	11678.5	12058.7	11232.9	11864.9	12106.5	**15745.3**	**15951.9**	**16144.4**	**16030.8**	**16903.1**	**6485.6**	**6384.7**	∞	**5926.5**	**1534.2**
F_{15}	11500.4	11577.5	11957.7	11131.9	11763.9	12005.5	**15644.3**	**15850.9**	**16043.4**	**15929.8**	**16802.1**	**6384.7**	**6485.6**	**5926.5**	∞	**1433.2**

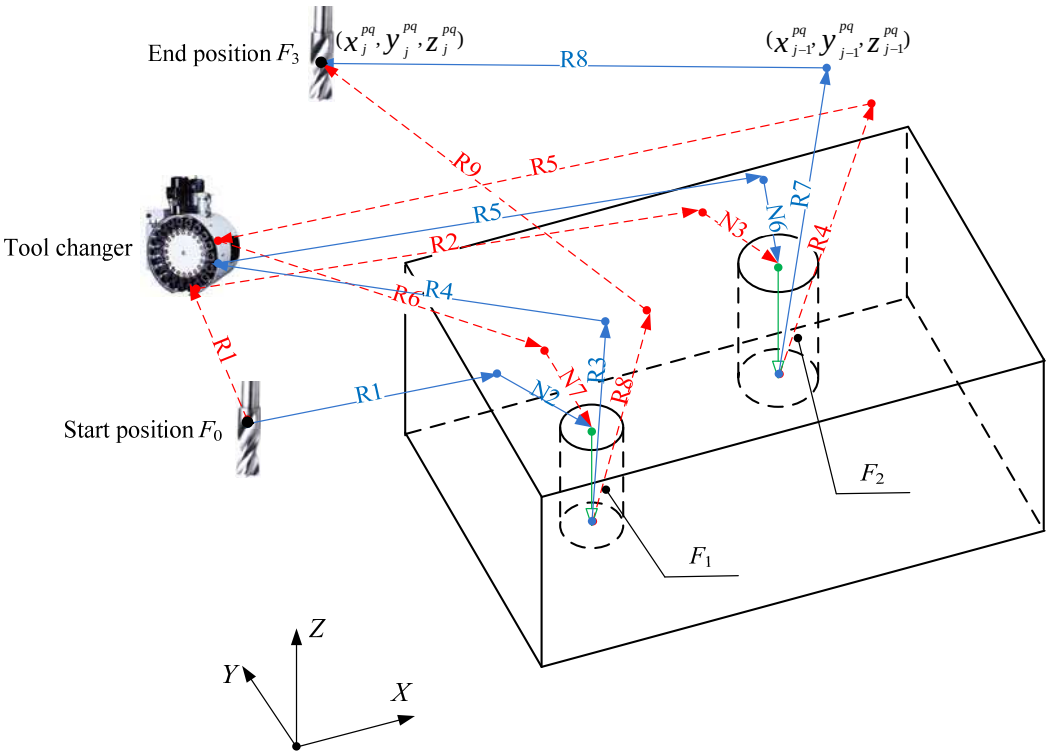

Fig. 1. A 2-feature part that has two feasible processing sequences.

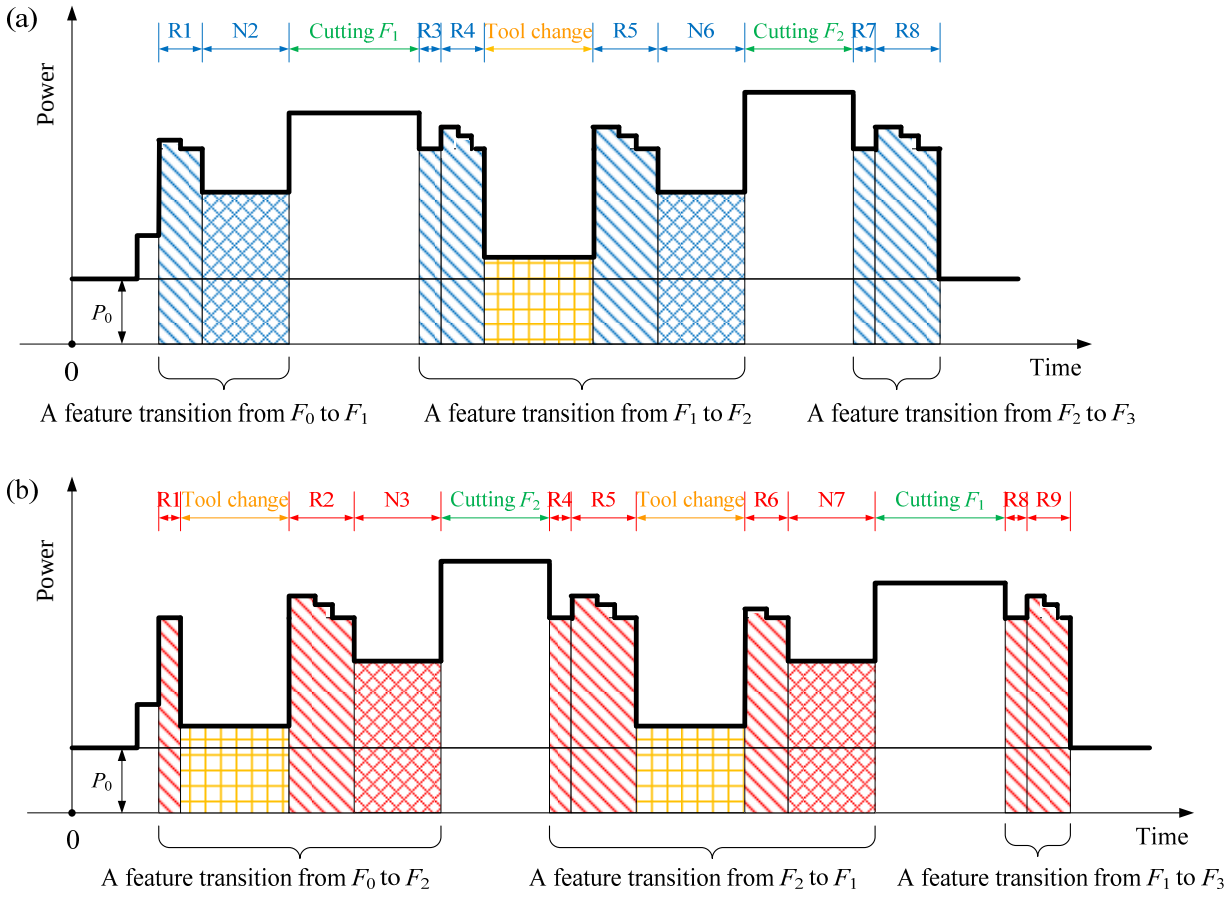

Fig. 2. Power profiles of two sequences: (a) F_0-F_1-F_2-F_3; (b) F_0-F_2-F_1-F_3.

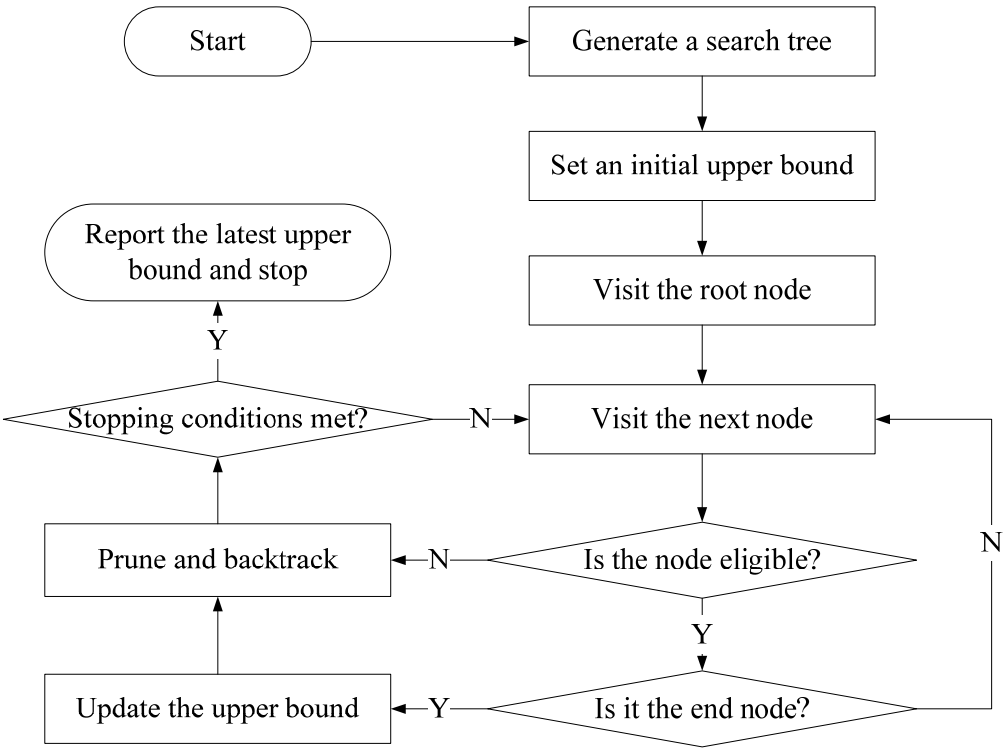

Fig. 3. A flowchart of depth-first search.

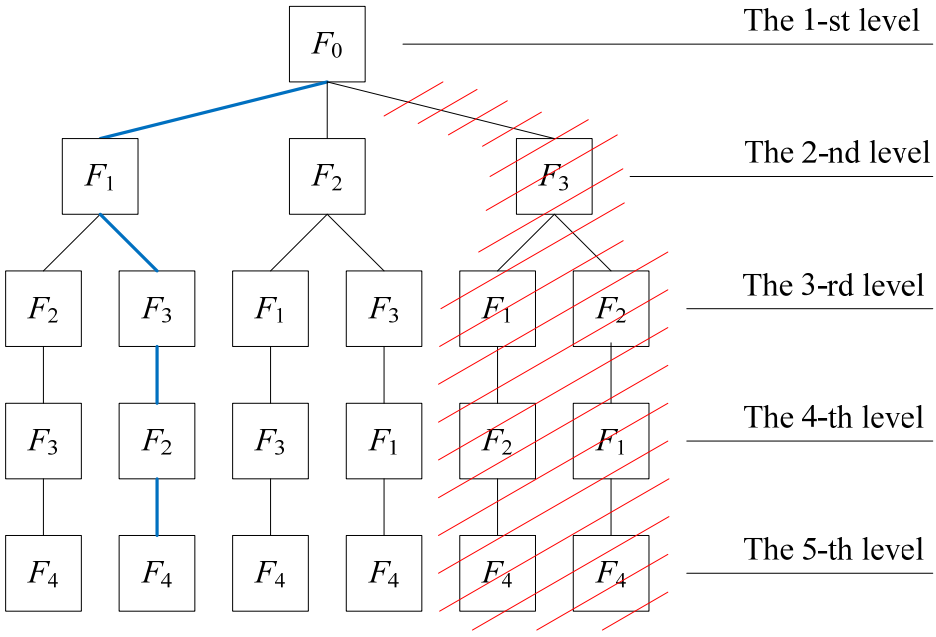

Fig. 4. The search tree for a 3-feature part.

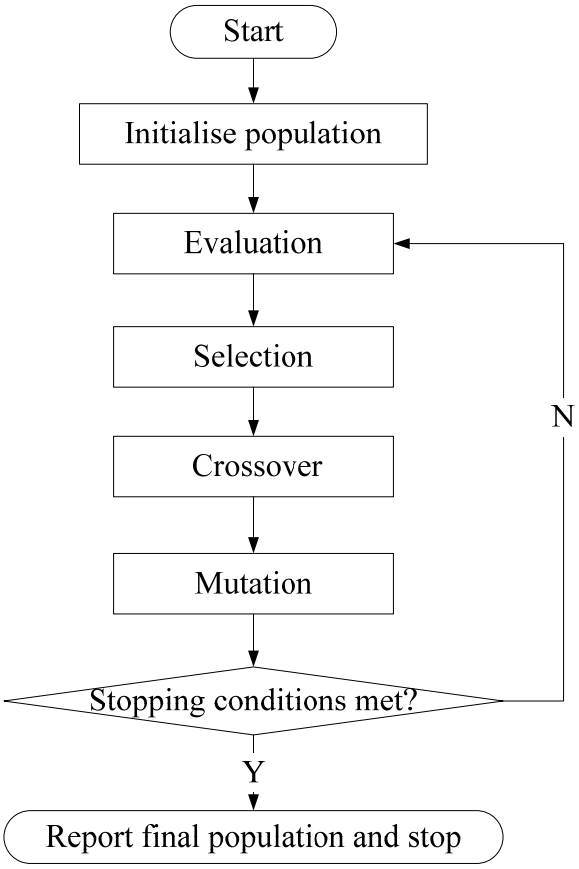

Fig. 5. A flowchart of genetic algorithm.

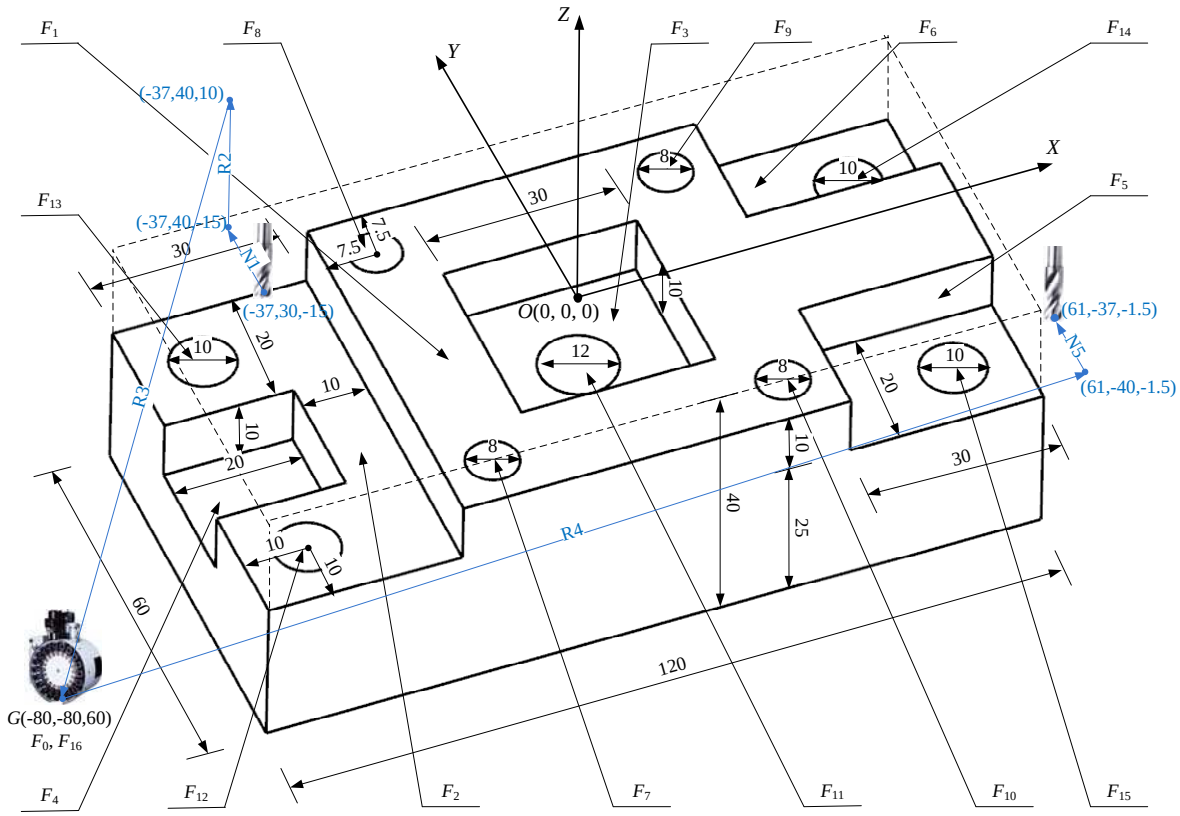

Fig. 6. A prismatic part with 15 actual features and 2 virtual features.

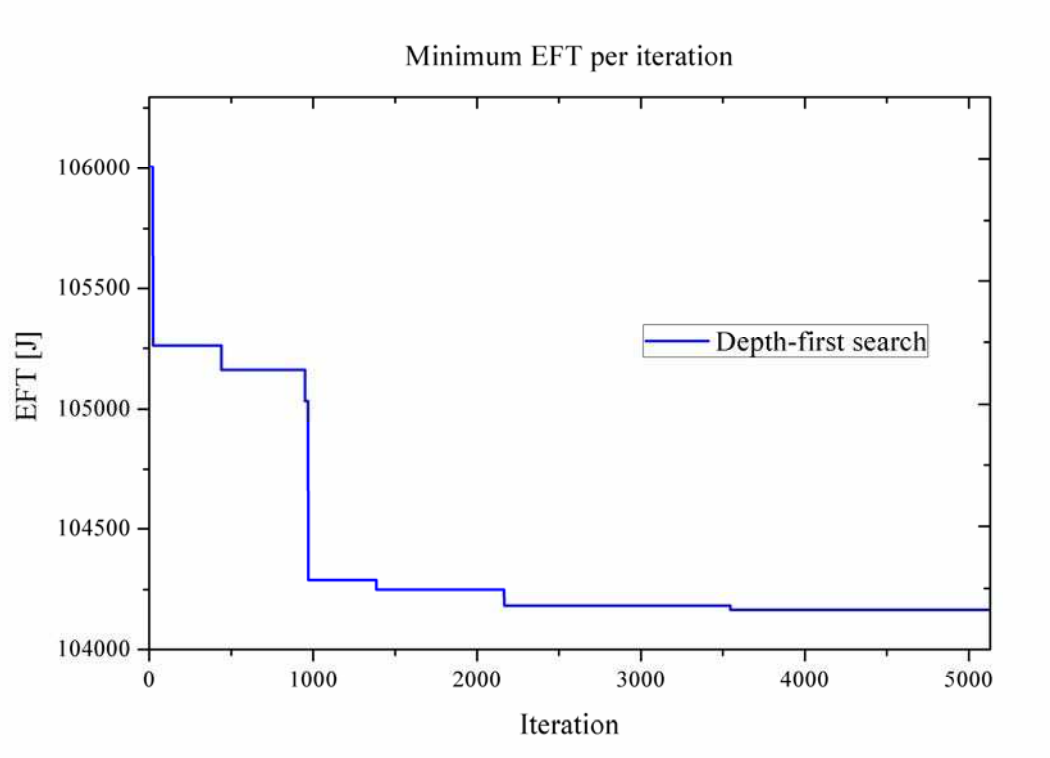

Fig. 7. The searching process of depth-first search for the optimal solution.

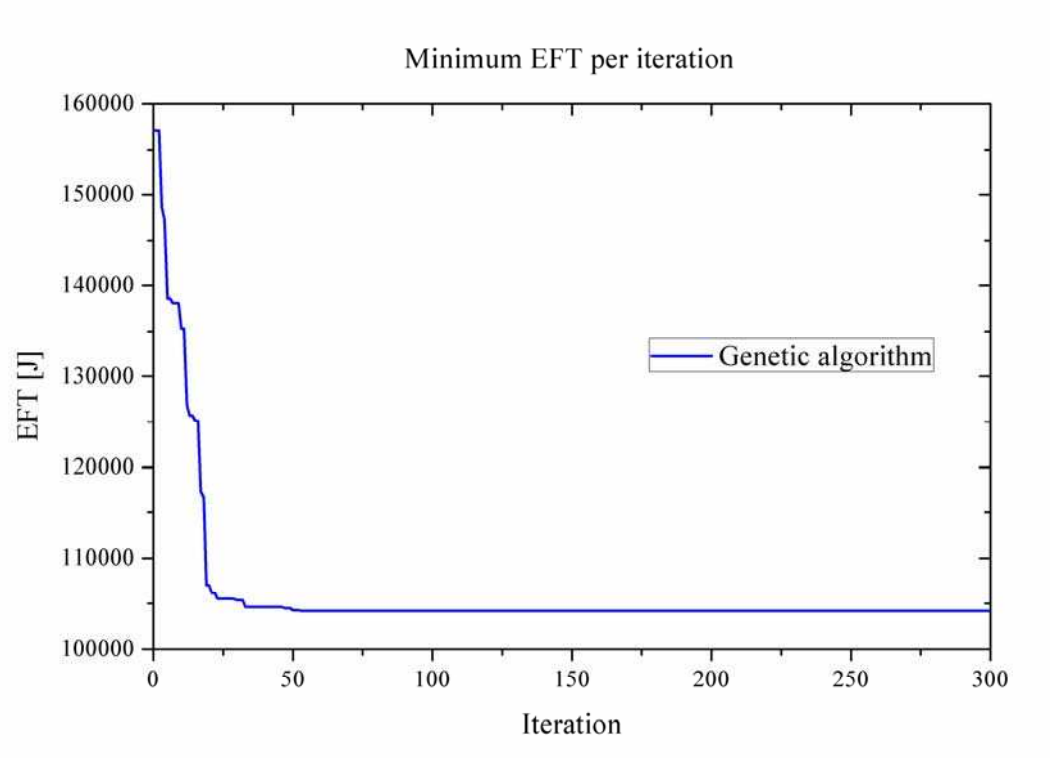

Fig. 8. A searching process of genetic algorithm for the optimal solution.

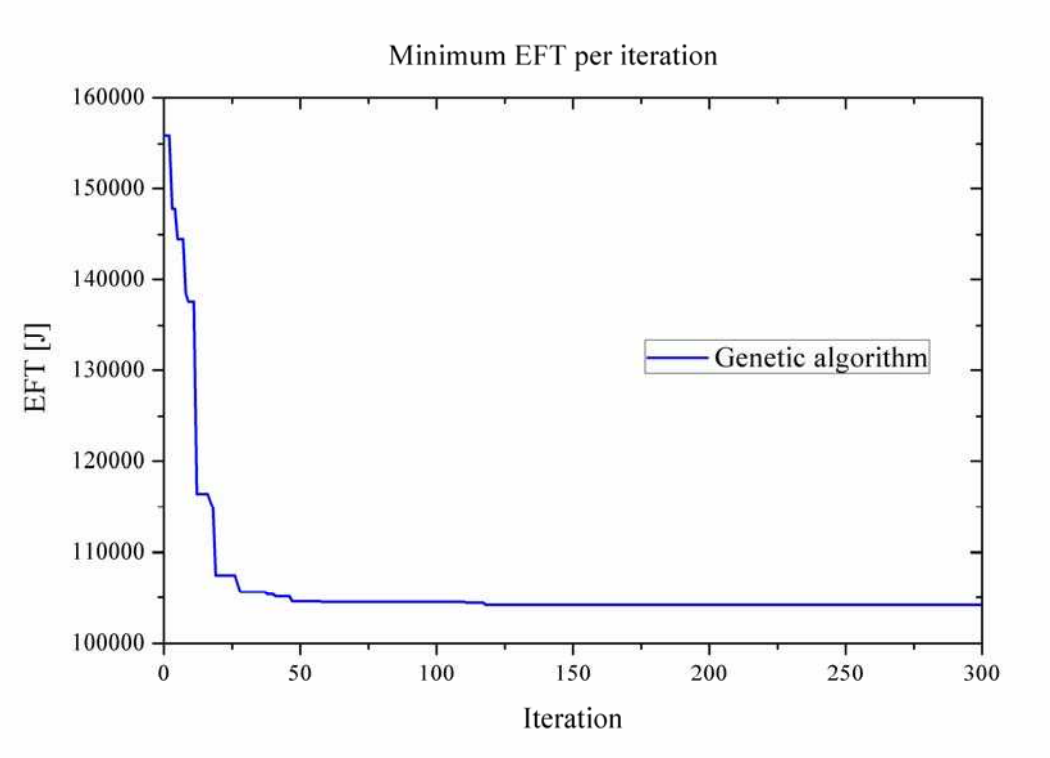

Fig. 9. A searching process of genetic algorithm for a near-optimal solution.